



Cosmochemical implications of CONSERT permittivity characterization of 67P/CG

Alain Hérique, Wlodek Kofman, Pierre Beck, Lydie Bonal, Ilaria Buttarazzi,
Essam Heggy, Jérémie Lasue, Anny Chantal Levasseur-Regourd, Eric Quirico,
Sonia Zine

► To cite this version:

Alain Hérique, Wlodek Kofman, Pierre Beck, Lydie Bonal, Ilaria Buttarazzi, et al.. Cosmochemical implications of CONSERT permittivity characterization of 67P/CG. Monthly Notices of the Royal Astronomical Society, 2016, 462 (Suppl. 1), pp.S516-S532. 10.1093/mnras/stx040 . insu-01452412

HAL Id: insu-01452412

<https://insu.hal.science/insu-01452412>

Submitted on 8 Mar 2017

HAL is a multi-disciplinary open access archive for the deposit and dissemination of scientific research documents, whether they are published or not. The documents may come from teaching and research institutions in France or abroad, or from public or private research centers.

L'archive ouverte pluridisciplinaire **HAL**, est destinée au dépôt et à la diffusion de documents scientifiques de niveau recherche, publiés ou non, émanant des établissements d'enseignement et de recherche français ou étrangers, des laboratoires publics ou privés.

Cosmochemical implications of CONSERT permittivity characterization of 67P/CG

A. Herique,^{1★} W. Kofman,^{1,2} P. Beck,¹ L. Bonal,¹ I. Buttarazzi,^{1,3} E. Heggy,⁴
J. Lasue,⁵ A. C. Levasseur-Regourd,⁶ E. Quirico¹ and S. Zine¹

¹Univ. Grenoble Alpes, IPAG, F-38000 Grenoble, France, CNRS, IPAG, F-38000 Grenoble, France

²Space Research Centre, PAN, Warsaw, Poland

³BRGM DAT/REU, Reunion Island Regional Office, F-97404 Saint-Denis, La Réunion Island, France

⁴University of Southern California, Ming Hsieh Department of Electrical Engineering, Viterbi School of Engineering, Los Angeles, CA 90089, USA

⁵Université de Toulouse; UPS-OMP; IRAP; CNRS; IRAP; 9 Avenue Colonel Roche, BP 44 346, F-31028 Toulouse Cedex 4, Toulouse, France

⁶UPMC (Sorbonne Univ.); UVSQ (UPSay); CNRS/INSU; LATMOS-IPSL, BC 102, 4 place Jussieu, F-75005 Paris, France

Accepted 2017 January 6. Received 2016 November 25; in original form 2016 June 14

ABSTRACT

Analysis of the propagation of the Comet Nucleus Sounding Experiment by Radiowave Transmission (CONSERT) signal throughout the small lobe of the 67P/CG nucleus has permitted us to deduce the real part of the permittivity, at a value of 1.27 ± 0.05 . The first interpretation of this value, using the dielectric properties of mixtures of ices (H_2O , CO_2), refractories (i.e. dust) and porosity, led to the conclusion that the comet porosity lies in the range 75–85 per cent. In addition, the dust-to-ice ratio was found to range between 0.4 and 2.6 and the permittivity of dust (including 30 per cent porosity) was determined to be lower than 2.9. This last value corresponds to a permittivity lower than 4 for a material without any porosity. This article is intended to refine the dust permittivity estimate by taking into account updated values of the nucleus densities and dust/ice ratio and to provide further insights into the nature of the constituents of comet 67P/CG. We adopted a systematic approach: determination of the dust permittivity as a function of the volume fraction of ice, dust and vacuum (i.e. porosity) and comparison with the permittivity of meteoritic, mineral and organic materials from literature and laboratory measurements. Then different composition models of the nuclei corresponding to cosmochemical end members of 67P/CG dust are tested. For each of these models, the location in the ice/dust/vacuum ternary diagram is calculated based on available dielectric measurements and confronted to the locus of 67P/CG. The number of compliant models is small and the cosmochemical implications of each of them is discussed, to conclude regarding a preferred model.

Key words: solid state: refractory – solid state: volatile – techniques: radar astronomy – comets: general – comets: individual: 67P/Churyumov-Gerasimenko.

INTRODUCTION

Rosetta is a European Space Agency (ESA) mission, dedicated to the study of comet 67P/Churyumov-Gerasimenko (thereafter 67P/CG). After a 10-year journey, *Rosetta* arrived at the comet in 2014 August and started its 26-month investigation to study the behaviour of the comet before, during and after perihelion. On 2014 November 12, *Rosetta*'s lander, Philae, was deployed at the surface. After the initial touchdown, Philae bounced several times before coming to rest (Biele et al. 2015). All scientific instruments were

activated during the First Science Sequence (FSS), until the batteries ran out of power on 2014 November 15. The location of the final landing site, initially unknown, has been narrowed down to a $106 \times 22 \text{ m}^2$ surface using Comet Nucleus Sounding Experiment by Radiowave Transmission (CONSERT) measurements (Herique et al. 2015). Philae was finally identified optically in 2016 September in the middle of this narrow area, just before the end of the *Rosetta* mission. CONSERT is a bistatic radar instrument designed to provide information about the deep interior of the comet by propagating long-wavelength electromagnetic waves between Philae and *Rosetta* (Kofman et al. 1998). After Philae's final landing at 17:31 UTC on 2014 November 12, CONSERT operated as initially planned from 18:56 UTC until 04:06 UTC on 2014 November 13

* E-mail: alain.herique@univ-grenoble-alpes.fr

and good measurements were obtained, leading to an estimation of the real part of the permittivity in the small lobe of the nucleus (Kofman et al. 2015).

The objective of this article is to put constraints on the estimate of the permittivity of the dust based on CONSERT measurements and to propose possible constituents for comet 67P/CG. Initially, we determine the possible range of dust permittivity as a function of the volume fraction of ice, dust and vacuum (i.e. porosity). We then compare this with the permittivities of meteoritic, mineral and organic materials from the literature and from laboratory measurements. Since many materials have similar permittivity values in our frequency range, using permittivity does not allow us to identify materials directly, but does allow us to exclude some. To this end, we test different composition models of the nucleus corresponding to cosmochemical end members of 67P/CG dust.

As usual for planetary sciences, the main difficulty is the lack of some information required to retrieve nucleus composition and especially the dielectric permittivities of nucleus constituent candidates measured in controlled and relevant environments. This first work is therefore based on measurements available in the literature, sometimes extrapolated or extended far from laboratory experimental conditions. We also highlight the missing relevant experimental data to provide a road map for cometary experimental work to be developed in the next few years in order to consolidate these preliminary results.

1. CONSERT 67P/CG PERMITTIVITY MEASUREMENT

An electromagnetic signal of about 3-m wavelength is transmitted from CONSERT on the *Rosetta* spacecraft in orbit around the nucleus. When CONSERT on the Philae lander located on the surface of the comet receives the signal, Philae transmits a second signal, which is, in turn, received by the orbiter. The time difference between transmitting and receiving the signal is carefully measured. It is a function of the relative position of *Rosetta* and Philae, but also depends on reflections and refractions within the nucleus. When the experiment was proposed in 1993 and according to understanding of the composition of cometary materials at that time, it was likely that propagation of electromagnetic waves of 3-m wavelength through the comet would be possible, so that a return signal would still be received even with Philae on the opposite side of the nucleus from the *Rosetta* orbiting spacecraft (Kofman et al. 1998).

The basic principle of the experiment is straightforward. An electromagnetic wave loses energy as it propagates through the cometary nucleus and travels at a smaller velocity than in free space. Both the actual amount of change in velocity and the energy loss depend on the complex permittivity of the cometary materials. They also depend on the ratio of the wavelength used to the size of any inhomogeneities present. Thus, any signal that has propagated through the medium contains information concerning this medium. As a result of a trade-off between the signal penetration, spatial resolution, antenna design, electronic speed, mass and power, we adopted a carrier frequency equal to 90 MHz, a bandwidth of 8 MHz and a sampling rate of 10 MHz (*I* and *Q* components). This bandwidth gives a resolution of 30 m in free space and less inside the comet nucleus, which is a satisfactory compromise between the scientific requirement and the technology. The major constraint, which is stability of the on-board clocks, led to the construction of the instrument working as a transponder in time between the *Rosetta* orbiter and the Philae lander (Kofman et al. 1998, 2007).

After the landing of Philae on the cometary surface, CONSERT operated over 9 hours during the First Science Sequence. The measurements explored the small lobe of the 67P/CG comet and allowed us to measure the dielectric properties of the cometary interior. The main results are as follows.

- (1) A rather homogenous nucleus on the scalelength of wavelengths (~ 25 cm–25 m), as no scattering of waves is observed down to -20 dB below the peak of the signal.
- (2) A real part of the permittivity, deduced from the propagation time, equal to 1.27 ± 0.05 .

These results have been obtained assuming that the bulk permittivity of the comet is constant on large scales. This assumption was necessary, as the exact localization of Philae was not yet known (Herique et al. 2015; Kofman et al. 2015). It allowed us, using the measurements for localization and propagation time, to determine the position of the lander Philae and the error with good accuracy. There is, of course, the possibility of a gradational variation of the dielectric properties along the propagation path. However, due to the length of propagation and a depth of penetration limited to about 100 m, the effect, if it exists, cannot be detected.

The localization of the lander in 2016 September will help us to analyse the CONSERT data better, all the more once future releases of the nucleus shape model are available. We are now starting to update the results presented in Kofman et al. (2015) and we expect limited implications on the average permittivity. This improved knowledge of both position and nucleus shape will allow us to study the spatial variability of the permittivity averaged along a propagation pass (Herique et al. 1999) and also to model the CONSERT lander antenna pattern to analyse the CONSERT received power (Hahnel et al. 2015). This future work is outside the scope of this article.

2. 67P/CG NUCLEUS COMPOSITION AND DIELECTRIC PROPERTIES

2.1 Temperature range

While the near-surface temperature at Philae during CONSERT operations is well known, the temperature inside the small lobe of the nucleus can only be approached through numerical modelling. Two of Philae's instruments provide information on the surface temperature. The temperature is within a 100–150 K range from SESAME data (Lethuillier et al. 2016) and about 90–130 K from MUPUS data (Spohn et al. 2015). Furthermore, the near-surface is likely to be a good insulator. The thermal inertia, as derived from MUPUS, is $(85 \pm 35) \text{ J m}^{-2} \text{ K}^{-1} \text{ s}^{-1/2}$ (Spohn et al. 2015), to be compared with a range of $10\text{--}50 \text{ J m}^{-2} \text{ K}^{-1} \text{ s}^{-1/2}$, derived from MIRO on board *Rosetta* for the overall subsurface (Gulkis et al. 2015). The interior of the nucleus is thus only weakly sensitive to variations in surface illumination, with temperatures most likely remaining below 100 K.

The primordial interior temperature of comet 67P at depth can be inferred from measurements of the cometary volatile species in 67P's coma. A typical value of around 30 K is determined from the different volatile species detected, including the nitrogen molecule N_2 (sublimation temperature 26–56 K, Rubin et al. 2015) and the oxygen molecule O_2 (20–30 K, Bieler et al. 2015). However, the depth at which the primitive material of 67P can be found is not well constrained. Based on one-dimensional thermal propagation models fitting the MIRO data, it has been determined that the diurnal variation in temperature is confined to the upper layer of the

Table 1. Dielectric permittivity of volatiles.

	ϵ	Frequency	Ref	Comments
H ₂ O hexa	3.1	90 MHz	Gough 1972	
H ₂ O amorphous	3.1–3.4	100 kHz	Andersson 2008	130 K
CO ₂	2.1	1 MHz	Pettinelli et al. 2003	200 K
CO	1.4	0.5–20 kHz	Pilla et al. 1999	42 K

Table 2. The volatile volume fraction models and corresponding density and permittivity ranges.

H ₂ O	CO ₂	CO	Density (kg m ⁻³)		Permittivity	
			Min	Max	Min	Max
94%	3%	3%	931	1171	3.0	3.3
75%	8%	17%	945	1138	2.7	3.0

subsurface, with a thermal penetration depth of a couple of centimetres. The thermal penetration depth linked to the eccentricity of the comet's orbit is likewise limited to the upper metres ($1/e$ attenuation of about 1 m, Gulkis et al. 2015). Assuming a homogeneous model for the comet and approximate values for the thermal properties of the cometary material, one can estimate the time propagation of the heat wave through the material using

$$\tau = \frac{d^2 \rho c_p}{k}, \quad (1)$$

where d is the depth of the base of the cryosphere, ρ the density of the material, c_p the heat capacity of the material and k the thermal conduction. Knowing that the thermal inertia of the material is

$$I = \sqrt{k \rho c_p}, \quad (2)$$

a typical depth of penetration for the heat wave is given by

$$d = \sqrt{\tau} \frac{I}{\rho c_p}. \quad (3)$$

We take the values determined by MIRO for the thermal inertia and assume that the density of the cometary material is about 500 kg m⁻³ and that the material has a heat capacity of around 500 J kg⁻¹ K⁻¹ (average heat capacity of meteorites at low temperature, Consolmagno et al. 2013). Then the depth range reached over a rotation of the comet is between 1 and 4 cm, while it is between 60 cm and 3 m for the orbital heat wave. We do not know how long the comet has been active, but a typical lifetime is considered to be around 10 000 years (Priyalnik et al. 2004), for which the penetration depth would range from 20–110 m. Therefore, it would be expected that primordial temperatures of the cometary interior would be reached a few tens of metres under the surface of the comet. This was also the conclusion of more elaborate numerical simulations of the thermophysical properties and heat-wave propagation in the subsurface of 67P (Lasue et al. 2008; De Sanctis et al. 2010; Rosenberg & Priyalnik 2010).

Thus, we can reasonably assume that the temperatures in the interior of the small lobe and in the near-surface at Abydos were below 150 K during FSS measurements and that the temperature decreases to reach a temperature lower than 70 K at a depth of a few tens of metres.

2.2 Composition of ices and expected permittivity

Cometary volatiles mostly consist of water, CO and CO₂. The contribution of other molecules, present at a much lower abundance of a few per cent (Ehrenfreund & Charnley 2000), is neglected here.

ROSINA revealed varying ratios between CO, CO₂ and H₂O, due to a heterogeneous coma, with expected higher CO and CO₂ mass flux from the southern hemisphere due to the seasonal illumination of the comet, which presents a high obliquity of 52° (Sierks et al. 2015). The ratios vary strongly with time and with the latitude and longitude of measurements (Hoang et al. 2017). The CO/H₂O number densities ratio is 0.13 ± 0.07 and the CO₂/H₂O ratio is 0.08 ± 0.05 in the last H₂O peak on 2014 August 7 (Hässig et al. 2015). Considering the values measured from the illuminated areas of the comet to be more representative of the bulk internal ratio of ices of 67P, VIRTIS-H and ROSINA measured an average CO₂/H₂O ranging from 0.02–0.07 and values of CO₂/H₂O typically below 0.02 (Bockelée-Morvan 2015; Le Roy et al. 2015). However, values as high as 0.60 for CO and 0.80 for CO₂ have been detected (Bockelée-Morvan 2015; Le Roy et al. 2015). They are located in non-illuminated parts of the comet, where the sublimation of water is reduced and the ratio of volatiles is probably not representative of the bulk composition of the comet. Moreover, measurements made in situ by Ptolemy at the Philae landing site confirm the range of CO/H₂O ratios to be from 0.03–0.10, but with a much higher CO₂/H₂O from 0.20–0.30 (Morse et al. 2015). However, these local values measured on an evolved part of the nucleus are not representative of its interior. At this point, it is very difficult to infer the actual bulk composition from coma measurements. Indeed, the production curves measured along the orbit, before and after perihelion, must be interpreted with models (Marboeuf & Schmitt 2014). In the present study, we test two composition scenarios: a volatile-rich comet with H₂O:CO:CO₂ = 75:17:08 per cent volume ratio (CO/H₂O number densities ratio = 0.13 and CO₂/H₂O = 0.07) and a volatile-poor comet with H₂O:CO:CO₂ = 94:2:3 per cent (CO/H₂O number densities ratio = 0.02 and CO₂/H₂O = 0.02) (Table 2).

The physical state of water ice in cometary nuclei is not firmly established either. It may be present in its hexagonal crystalline phase and amorphous phase, as postulated in Klinger et al. (1996) and Festou, Keller & Weaver (2004). The permittivity (Table 1) of hexagonal water ice at low temperature is 3.1 at 90 MHz (Gough 1972) and its density is 919 kg m⁻³ at 273 K, slightly increasing with decreasing temperature up to 934 kg m⁻³ at 93 K (Lide 2005). The permittivity of amorphous water ice ranges between 3.1 and 3.4 at 100 kHz (Andersson 2008). We can expect similar values at 90 MHz, as crystalline or amorphous water ice are not dispersive for frequencies in the range from kHz to GHz. The density of amorphous water ice is then 940 kg m⁻³ for low-density amorphous ice and 1170 kg m⁻³ for high-density amorphous ice (Watanabe & Kouchi 2008).

In the literature, the permittivity of CO_2 is given as 2.1 at 200 K in the 1-MHz frequency range (Pettinelli et al. 2003), with a density equal to 1512 kg m^{-3} at 216.4 K, and the permittivity of CO is given as 1.42 at 4.2 K, near-constant in the range from 5–20 kHz (Pilla et al. 1999) with a density of 800 kg m^{-3} .

Table 2 summarizes the two extreme scenarios we consider in this study. For each one, we assume the ice mixture as the juxtaposition of separate phases to estimate the effective permittivity using mixing formulae (Hashin–Shtrikman bounds, as discussed in Section 3). Values of the water ice permittivity (amorphous versus hexagonal) are therefore used to give extreme values of the volatile fraction permittivity; the permittivity ranges from 2.7–3.0 for the CO/ CO_2 -rich mixture and from 3.0–3.3 for the other. To analyse our data, we then take extreme permittivity values 2.7 and 3.3 and we also consider a mid-range permittivity case equal to 3.0. These models also give the density based on the hypothesis of separate phases and using the ice density discussed above. The resulting ranges are almost equal for the two models, in as far as the main unknown comes from the water ice density (I_h , HAD, LDA). We then consider a density ranging from 937 – 1171 kg m^{-3} : this upper limit is obtained assuming that water ice is only constituted of high-density amorphous ice, which in the context of cometary material is probably not a very realistic case, due to the condensation conditions of the protoplanetary nebula.

2.3. Composition of the refractory component

The composition of the refractory and semi-refractory component is more difficult to assess than for the ices, which can be analysed in the coma after their sublimation (see Cochran et al. 2015 for a review). Before the results of the *Rosetta* mission, cometary flybys had already established that cometary nuclei are rich in both minerals (mostly silicates) and a heterogeneous and unequilibrated distribution of refractory organic compounds (Kissel et al. 1986; Brownlee, Joswiak & Matrajt 2012). Besides this, remote observations in the infrared domain have provided clues to the presence of amorphous and crystalline silicates (Kelley & Wooden 2009), while remote polarimetric observations have provided clues to the presence of a significant fraction of absorbing organics (Levasseur-Regourd, Zolensky & Lasue 2008). The composition of the organic component has been suggested to be similar to that of some interplanetary dust particles collected in the stratosphere (so-called IDPs). The cosmochemical implications are deeply discussed in Section 4.

2.4 Density and porosity

The bulk density of a nucleus is derived from its mass, indirectly estimated from non-gravitational force modelling, and its mean size, tentatively derived from remote observations. For comet 67P/CG, masses from 3.5×10^{12} to $1.6 \times 10^{13} \text{ kg}$ have been proposed by Davidsson & Gutiérrez (2005) based on non-gravitational force effects. Mean effective sizes of the nucleus of about 4 km have been proposed: $(3.96 \pm 0.04) \text{ km}$ by Lamy et al. (2007) based on *Hubble Space Telescope* (HST) observations and $(4.08 \pm 0.22) \text{ km}$ by Kelley et al. (2009) from *Spitzer* observations. Such results correspond to a very low density (below 500 kg m^{-3}); they could suggest the existence of sub-nuclei and fractures, as well as an intrinsic porosity of the refractory component (in agreement with clues from the structure of dust in the coma) and possibly also of the ices (Levasseur-Regourd et al. 2009).

Since the *Rosetta* rendezvous mission, the mass (or more exactly the product of the mass by the gravitational constant) is derived

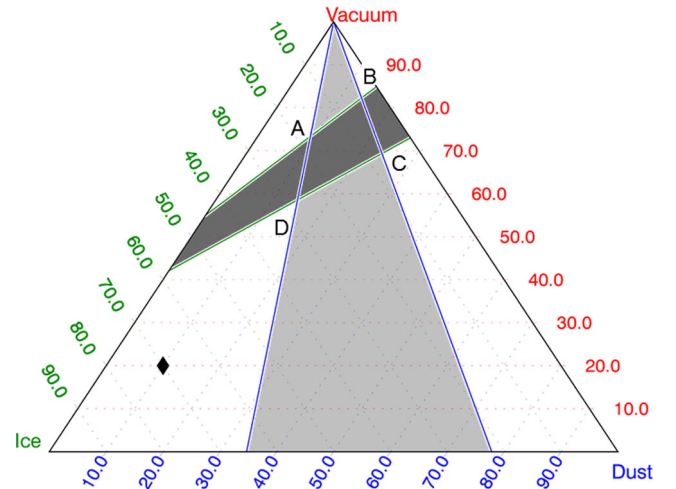


Figure 1. Ternary diagram as a function of the volume percentage of ice fraction, dust fraction and vacuum fraction (porosity), given domains limited by the ice-to-dust volume ratio model (grey) and density model (dark grey), given our Domain of Interest (DoI: quadrilateral ABCD). To help the reader unfamiliar with ternary diagrams, the black diamond is displayed as an example corresponding to 10 per cent dust, 70 per cent ice and 20 per cent vacuum (or porosity).

from radio science investigations (Pätzold et al. 2007), while the volume is obtained from a shape model. The first direct estimation of mass was $1.0 \times 10^{13} \text{ kg}$, while the density, from a shape model built while the South Pole was still in shadow, was $(470 \pm 45) \text{ kg m}^{-3}$ (Sierks et al. 2015). With a higher resolution shape model, the density was found to be $(535 \pm 35) \text{ kg m}^{-3}$ (Preusker et al. 2015). Further analyses, with even more accurate estimations of the mass and the shape as the southern hemisphere was illuminated by the Sun, converge towards a density of $(533 \pm 6) \text{ kg m}^{-3}$ (Pätzold et al. 2016). There is no clue pointing to differences of densities between the two lobes of the nuclei, as the gravity field remains homogeneous for distances above 10 km between the centre of mass and *Rosetta*. However, more results are expected from the 2016 September observations, with orbits reaching altitudes below 1 km, during the slow final descent of *Rosetta* to the nucleus.

The ternary diagram in Fig. 1 compiles the constraints deduced from the density (dark grey polygon). One point on the diagram corresponds to a given ice (i.e. mixture of ices as discussed in Section 2.2 and Table 2), dust and vacuum (i.e. porosity) volume ratio (Kamoun et al. 2014; Kofman et al. 2015). Dust and ice materials are considered without any internal porosity at micro- or macrometre scales: internal porosities at any scale contribute to the vacuum volume ratio. One issue is to localize the bulk properties of comet 67P/CG precisely in this diagram. Only a restricted area is found to be compliant with the values of these three parameters constrained by the *Rosetta* mission (ABCD polygon in Fig. 1).

The ice density range has been estimated as $(1051 \pm 120) \text{ kg m}^{-3}$. The composition of the dust fraction will be discussed further in Section 4, but for now we consider that the dust density, *without porosity*, ranges from 2000 – 3500 kg m^{-3} . These values allow us to calculate the range of density corresponding to each point on the ternary diagram. Then the density constraints from radio science (Table 3) limit the domain of acceptable volume ratio in our ternary diagram, as plotted in Fig. 1 in dark grey: the width of this domain is due mainly to the uncertainty in the dust density and will be reduced by mineralogical constraints.

Table 3. Density as a function of measured average density of the comet and assumed grain density, taking into account the uncertainties in density determination. (In bold the extreme values as reported in ternary diagrams are shown – see Fig. 1).

Density (kg m ⁻³)	Ice density (kg m ⁻³)	Dust density (kg m ⁻³)	Ice fraction (%)	Dust fraction (%)	Porosity (%)
527	1171 931	3500	0.0	15.1	84.9
		2000	0.0	26.4	73.7
			45.0	0.0	55.0
			56.6	0.0	43.4
539	1171 931	3500	0.0	15.4	84.6
		2000	0.0	27.0	73.0
			46.0	0.0	54.0
			57.9	0.0	42.1

Table 4. Dust/ice volume fraction as a function of the D/I mass ratio and density hypothesis.

Ice (density)	Dust (density)	Dust/ice mass	Dust/ice vol	Dust/(ice+dust) vol fraction %
931	3500	2	0.53	34.7
931	2000	2	0.93	48.2
1171	3500	2	0.67	40.1
1171	2000	2	1.17	53.9
931	3500	4	1.06	51.5
931	2000	4	1.86	65.1
1171	3500	4	1.34	57.2
1171	2000	4	2.34	70.1
931	3500	6	1.60	61.5
931	2000	6	2.79	73.6
1171	3500	6	2.01	66.7
1171	2000	6	3.51	77.8

2.5 Dust-to-ice ratio

The dust-to-gas ratio in comets is an important parameter, as it can be used to classify comets from ground-based observations (A’Hearn et al. 1995; Mumma & Charnley 2011), even if observed values depend on a number of assumptions (grain-size distribution and densities; physical properties of the comets, etc.). From ground-based observations, the dust-to-ice mass ratio of 67P/CG was observed to vary over a large range from relatively low values (0.5–1.75; Hanner et al. 1985; Krishna Swamy 1991) to higher values 3–4.8 (Fulle et al. 2004; Weiler et al. 2004). Better constraints on these parameters were obtained after *Rosetta*’s rendezvous from a combination of measurements with GIADA and OSIRIS dust detections and MIRO and ROSINA instruments for the quantification of the volatile content of the nucleus. Using these different measurements, the dust-to-gas mass ratio of 67P/CG was inferred to be approximately 4 ± 2 averaged over the sunlit nucleus surface (Rotundi et al. 2015), confirming the relatively dusty nature of the comet. Since the beginning of the mission, this measurement has remained relatively consistent and likely reflects the properties of the material ejected from the comet. The bulk interior properties may be different, as the ejected material could be more processed than the pristine deep interior.

With this refined estimation of ice density and the enlarged range of dust density, a dust-to-ice mass ratio of 4 ± 2 corresponds to a dust/(ice + dust) volume ratio ranging from 35–78 per cent. This ratio corresponds to the dust ratio of the solid fraction of the nucleus and defines an additional domain in our ternary diagram (Fig. 1, in grey, and Table 4). Only the intersection of the two grey and dark-grey triangles is compliant with the constraints on the density and dust-to-ice ratio coming from other *Rosetta* instruments. We will

therefore consider this area as our ‘domain of interest’ (DoI) to be analysed further with CONCERT’s permittivity estimation.

3. PERMITTIVITY OF THE DUST FRACTION

Kofman et al. (2015) compared the CONCERT permittivity with laboratory measurements of the permittivity of ordinary and carbonaceous chondrites, to exclude ordinary chondrites as a potential cometary dust analogue. Our reanalysis of the density and composition of 67P/CG does not question this result. From this measurement, we first derive the dust permittivity as a function of the ice/dust/vacuum volume fractions and of ice permittivity. We then derive constraints on the dust composition.

The effective permittivity of a mixture is known to be highly sensitive to the applied mixing formula and many formulae are described in the literature (Sihvola 1999). A conservative approach is to take the Hashin–Shtrikman bounds (HS1 and HS2), which correspond to theoretical permittivity upper and lower bounds for an isotropic mixture of two phases without chemical interactions (Sihvola 1999):

$$\varepsilon_{\text{HS1}} = \varepsilon_e + 3f\varepsilon_i \frac{\varepsilon_i - \varepsilon_e}{\varepsilon_i + 2\varepsilon_e - f(\varepsilon_i - \varepsilon_e)}, \quad (4)$$

$$\varepsilon_{\text{HS2}} = \varepsilon_i + 3(1-f)\varepsilon_e \frac{\varepsilon_e - \varepsilon_i}{\varepsilon_e + 2\varepsilon_i - (1-f)(\varepsilon_e - \varepsilon_i)}, \quad (5)$$

where ε_e is the permittivity of the embedded medium and ε_i and f are the permittivity and volume fraction of the inclusions. These bounds cover all the geometries in terms of inclusion shape and size, assuming an isotropic distribution. In our three-phase media,

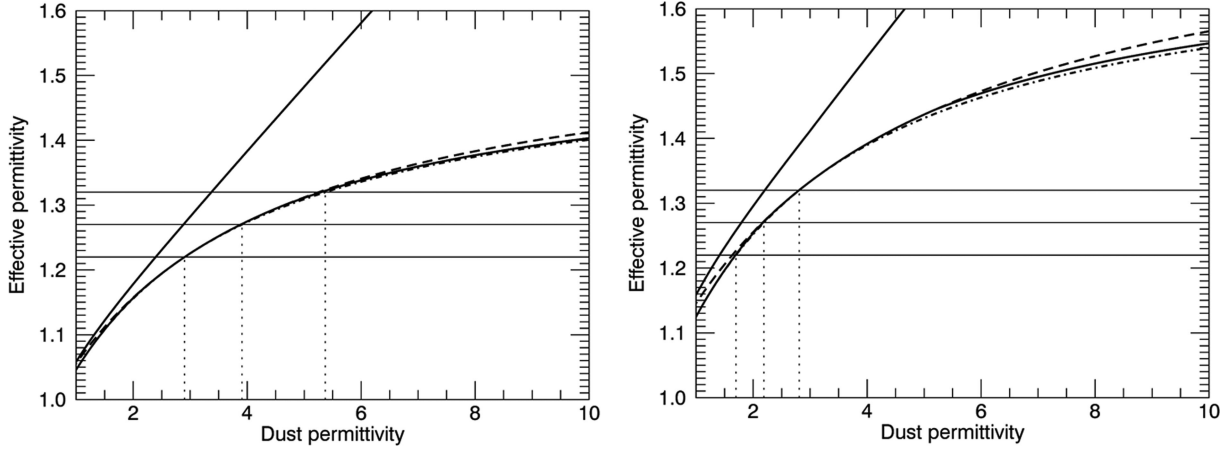


Figure 2. Effective permittivity of nucleus versus dust permittivity for a mixture of ice ($\epsilon = 3.0$), dust and porosity, using the three-phase Maxwell–Garnett mixture formula (dash–dotted line), layered–sphere mixture formula (dashed line) and Hashin–Shtrikman bounds (solid lines). Left: 82.3 per cent porosity, 3.9 per cent ice ($\epsilon = 3.0$) and 13.7 per cent dust (extreme case, upper right corner of DoI). Right: 75 per cent porosity, 10 per cent ice ($\epsilon = 3.0$) and 15 per cent dust. Horizontal lines give CONSERT measured permittivity range = 1.27 ± 0.05 and vertical dotted lines indicate the corresponding dust permittivity for MG3, LS and HS–min.

we apply the bounds for the different phases recursively to take the maximum and minimum permittivity.

In addition to these bounds, we consider two other models based on some assumptions on the geometry of the ice and dust distribution. We applied the well-known Maxwell–Garnett model for a three-phase mixture (MG3) with spherical inclusions of permittivity ϵ_1 and ϵ_2 (volume fraction f_1 and f_2 respectively) embedded in a medium ϵ_e (vacuum portion, $\epsilon_e = 1$) (Sihvola 1999):

$$\epsilon_{\text{MG3}} = \epsilon_e + 3\epsilon_e \frac{f_1 \frac{(\epsilon_1 - \epsilon_e)}{\epsilon_1 + 2\epsilon_e} + f_2 \frac{(\epsilon_2 - \epsilon_e)}{\epsilon_2 + 2\epsilon_e}}{1 - \left(f_1 \frac{(\epsilon_1 - \epsilon_e)}{\epsilon_1 + 2\epsilon_e} + f_2 \frac{(\epsilon_2 - \epsilon_e)}{\epsilon_2 + 2\epsilon_e} \right)}. \quad (6)$$

This classical model is relevant, considering the high porosity, and assumes a separation of the ice and dust inclusions and their spherical shapes. We can expect limited deviation with regards to the lower HS bounds, which corresponds to the Maxwell–Garnett two-phase formula corresponding to a spherical inclusion in a vacuum. Another model consists of a layered sphere (LS) with a sphere of dust (ϵ_2, f_2) covered by a layer of ice (ϵ_1, f_1) and embedded in a medium ϵ_e (vacuum) (Sihvola & Lindell 1989; Sihvola 1999):

$$\epsilon_{\text{LS}} = \epsilon_e + 3\epsilon_e \frac{\frac{(f_1 + f_2)^2 (\epsilon_1 - \epsilon_e)(\epsilon_2 + 2\epsilon_1) + f_2 (2\epsilon_1 + \epsilon_e)(\epsilon_2 - \epsilon_1)}{(f_1 + f_2)(\epsilon_1 + 2\epsilon_e)(\epsilon_2 + 2\epsilon_1) + 2f_2 (\epsilon_1 - \epsilon_e)(\epsilon_2 - \epsilon_1)}}{1 - \frac{(f_1 + f_2)^2 (\epsilon_1 - \epsilon_e)(\epsilon_2 + 2\epsilon_1) + f_2 (2\epsilon_1 + \epsilon_e)(\epsilon_2 - \epsilon_1)}{(f_1 + f_2)(\epsilon_1 + 2\epsilon_e)(\epsilon_2 + 2\epsilon_1) + 2f_2 (\epsilon_1 - \epsilon_e)(\epsilon_2 - \epsilon_1)}}. \quad (7)$$

This latter model currently corresponds to the most relevant geometry by which to model primitive cometary material originating from the ice condensation around refractory grains (Li & Greenberg 1997).

Fig. 2 shows the mixture effective permittivity as a function of the dust permittivity for the different mixture formulae and for two distinct volume ratios. The horizontal lines limit the range of comet permittivity as measured by CONSERT: 1.27 ± 0.05 . In this domain, the graph shows that the effective permittivity is nearly equal when calculated by MG3, LS and the lower HS bound. This is the case for our whole domain of interest in terms of volume ratio and permittivities. We will therefore consider only the two

HS bounds for further analysis. The difference between the two HS bounds comes from the geometry and we expect the lower bounds to be closer to the true value for material with large porosity (>60 per cent in our domain of interest). Indeed, the geometry corresponding to the lower bounds with the vacuum taken as the matrix is more realistic for a comet. It is the same for MG3 and LS geometries, with upper bounds taking the porosity as inclusions and underestimating the permittivity.

For a given formula, this graph allows us to retrieve the constraints set by CONSERT: a comet permittivity equal to 1.27 ± 0.05 thus limits the dust permittivity to the 2.9–5.4 range, considering the lower HS bounds, a given volume ratio [porosity 82.3 per cent/ice 3.9 per cent/dust 13.7 per cent] and $\epsilon_{\text{ice}} = 3.0$ (Fig. 2, left). The higher estimated permittivity (higher HS bound) gives the lower estimation of the dust permittivity and vice versa. In practice, as shown in Kofman et al. (2015), we have to find refractory material with permittivity values low enough to fit with CONSERT measurements. Then, the main constraint to discriminate between different dust materials is the upper limit of the dust permittivity range, given by the lower HS bound. The higher HS bound indicates values close to 1 in a large part of our domain of interest (Fig. 2, right), adding no additional constraints. For further analysis, we will focus mainly on the lower HS bound to estimate dust permittivity. Estimated permittivity values are plotted on a ternary diagram in Fig. 3(a) for the lower bound with 67P/CG permittivity equal to 1.27 and an ice permittivity equal to 3.0. Drawn permittivity values are limited at $\epsilon = 5$ in order to optimize the colour scale for the area of interest and the plot is then saturated in the upper part of the diagram in red. The diagram shows a radial structure organized around one point (20 per cent ice, 0 per cent dust and 80 per cent porosity): for the applied mixing formula, this is the volume ratio (pure porous ice) for which the effective permittivity equals the CONSERT measurement and all the plotted equipermittivity domains converge to this point.

The diagram presents a large ‘forbidden area’: the black domain corresponds to retrieved permittivity values lower than 1, impossible for any expected material. In this way, CONSERT provides a new constraint on the ice/dust ratio and possible densities. We will discuss later how the purple and dark-blue domains, with permittivity values lower than 1.5 and 2 respectively, also appear unrealistic with regards to the candidate materials.

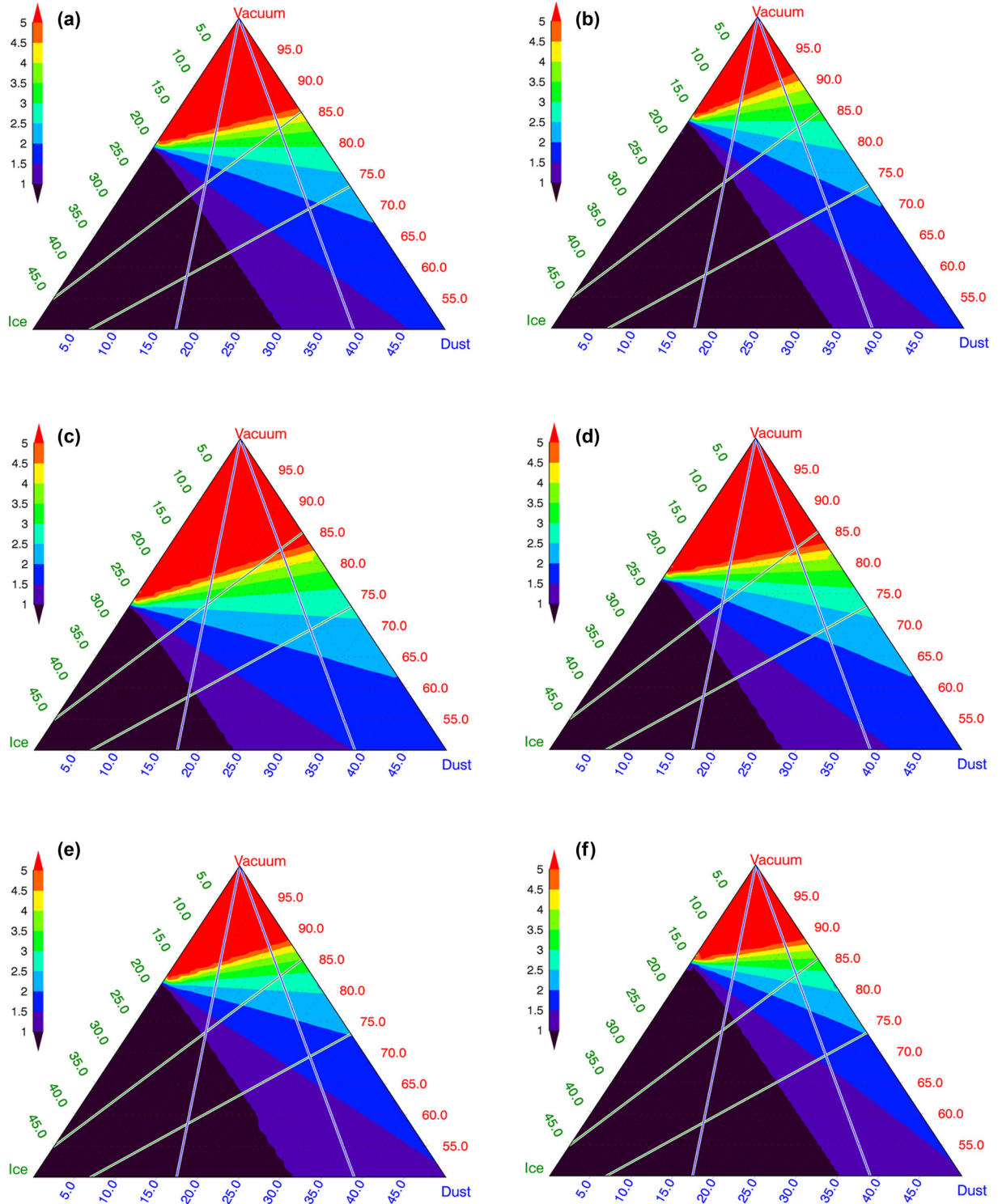


Figure 3. Ternary diagram given the dust permittivity estimated from the Hashin–Shtrikman bound as a function of the ice/dust/vacuum volume ratio and for 67P/CG permittivity measured by CONSERT and different models of ice permittivity.

The following diagrams allow coverage of the range of uncertainties in retrieved permittivity values. As previously noted, the higher HS bound in Fig. 3(b) underestimates the permittivity: the difference between higher and lower HS bound permittivity estimates is lower than 1 in our domain of interest.

Fig. 3(c)–(f) quantifies the effects of CONSERT accuracy and ice modelling: the position of the convergence centre for pure porous

ice is shifted by the 67P/CG permittivity or ice permittivity, as previously explained. Our domain of interest and also the impossible ‘black domain’ exclude very low dust/ice. The ice permittivity has a limited impact on the retrieved permittivity, inducing an inaccuracy lower than 1 (min/max). On the other hand, the effect of CONSERT measurement uncertainties is larger and reaches 2.4 (min/max) in the upper right corner of our domain of interest (Point B in Fig. 1).

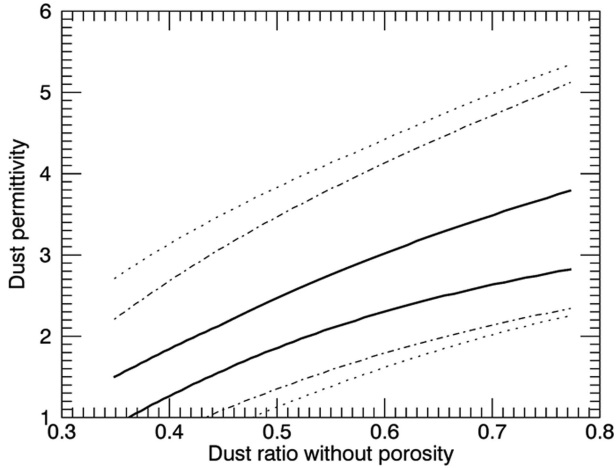


Figure 4. Dust permittivity (ϵ) along the upper limit of our domain of interest (nucleus density = 527, dust density = 3500, i.e. segment A–B in Fig. 1) as a function of the dust ratio without porosity (i.e. $D/(I+D)$ volume ratio). HS bounds for measured $\epsilon = 1.27$ with ice permittivity $\epsilon = 3.0$ (continuous line); for $\epsilon = 1.27 \pm 0.05$ with ice $\epsilon = 3.0$ (dashed line) and $2.7/3.3$ (dotted line).

In an unexpected way, this last term is the main error term in the inversion process, larger than the permittivity retrieval uncertainties: this corresponds to a specific range of volume ratios and cannot be generalized in any way.

To summarize, maximum dust permittivity is given by the low HS bound with the upper limit of the CONSERT measurement and the lower limit of the ice permittivity (Fig. 3(c), $\epsilon_{\text{CONSERT}} = 1.32$ and $\epsilon_{\text{ice}} = 2.7$). The lower limit is not really significant and is given by the high HS bound for CONSERT minimum value and ice maximum value (not plotted).

The estimated dust permittivity values are low in the DoI. This analysis makes it difficult to consider porosity values lower than about 65 per cent, especially when the associated dust-to-ice mass ratio is lower than 3. The maximum value of the permittivity corresponds to the upper limit of the dust-to-ice ratio. Then the dust permittivity is lower than 5.4, but this value is an extremum, in the upper right corner of our domain of interest (Fig. 3c), and the permittivity decreases drastically when we deviate from this extreme case (Fig. 4). This upper right corner corresponds to a dust/ice/porosity volume ratio with all considered uncertainties pushing in the same way: uncertainties in the permittivity estimation (CONSERT measurement, ice permittivity) but also uncertainties on the DoI in the ternary diagram consisting of the dust-to-ice ratio, comet density and constitutive material density. These last terms can be refined by confrontation of the estimated permittivity with the known permittivity and density of minerals and organic material.

4. FROM PERMITTIVITY TO MINERALOGY

The permittivity of different materials and mixtures of materials can be compared with the dust permittivity range deduced from CONSERT. In other words, we have excluded materials or mixtures with a permittivity larger than 5.4 (Table 5; Tables A1 and A2 in Appendix). What is the significance of this limit? The dust component is expected to be a mixture of organics and minerals, for which the resulting permittivity is an ‘average’ value depending on both the permittivity and relative abundances of each constituent. The dust fraction has to contain a fraction of low-permittivity materials in order to have an equivalent permittivity compliant with

CONSERT measurements. Materials with high permittivity (> 5.4) can be present if their presence is balanced by other materials with lower permittivity. For instance, olivine ($\epsilon \approx 6.8$) can contribute up to 40 per cent maximum if it is associated with quartz ($\epsilon \approx 4.6$), to be compliant with our limit $\epsilon = 5.4$. However, it can contribute up to 80 per cent when associated with coal materials ($\epsilon \sim 2.0$).

In this study, we have used the permittivity values reported in the literature. A major issue arises from these data due to the heterogeneity of experimental conditions under which measurements were collected. This includes samples physical properties, preparation, measurement method and frequency range. Of particular interest is the sample porosity, as measurements performed on minerals and meteorite powders include some porosity. The permittivity of a porous material is lower than that of the corresponding dense material and permittivity values might thus be underestimated. Note that meteorites contain an intrinsic porosity, due to the fine-grained nature of the matrix and, to a lesser extent, cracks and voids due to shock processes. Ordinary chondrites have typical porosities of just under 10 per cent, while carbonaceous chondrites tend to be more than 20 per cent porous (Consolmagno, Britt & Macke 2008). Meteorite permittivity therefore allows for a comparison with the bulk rock, but not directly with the mineralogical composition.

Kofman et al. (2015) considered the permittivity of meteoritic materials including porosity, initially and after the volume fractions of the different phases were normalized. This approach requires knowledge of the porosity. Unfortunately, this parameter is not often known, and a large proportion of the published permittivity values are not porosity-corrected. In this study, our analysis has been performed taking into account the contribution of porosity through another approach. It consists of calculating the permittivity of the material without any porosity using HS bound calculations from experimental measurements, for which the porosity of studied samples is known. This increases the uncertainty interval by using the HS formula twice, but allows the comparison of different materials. In practice, we considered mainly the lower HS bound treatment, which underestimates the permittivity. In cases in which the porosity was unknown, the measured permittivity was used without any correction, providing underestimated permittivities. Both lower HS bounds and uncorrected porosity are biased, because they underestimate the true permittivity value of the sample: the permittivity used can be lower than our limit, while the true and unknown permittivity is higher, but the inverse case is not possible. In other words, we can undeservedly preserve some materials but cannot wrongly exclude them. This approach allows us to build a list of possible candidates (i.e. not excluded), to be consolidated by further work and especially by laboratory measurements in relevant conditions of temperature and frequency.

Below, we compile literature data and critically discuss their relevance for the interpretation of CONSERT data.

4.1 Measured permittivity of meteoritic material

Meteorites are divided into two main categories – chondritic and non-chondritic meteorites – based on their bulk compositions and textures. Chondrites escaped differentiation and melting and are thus the meteorites with the best preserved materials originally present during their formation. Non-chondritic meteorites (such as mesosiderites) lack chondritic textures and were formed by partial or complete melting and planetary differentiation of chondritic precursor asteroids or larger planetary bodies.

Chondrites are further classified into three classes, among which are ordinary chondrites and carbonaceous chondrites. Classes are

Table 5. Dielectric permittivity of meteoritic materials measured including porosity and permittivity range after correction of the porosity when known. epsilon: real permittivity; tan delta: loss tangent (in bold: meteorites compliant with the CONSERT permittivity).

Meteorites	Without porosity		ϵ	Measured with porosity		Frequency (MHz)	Reference	Meteorite name	Temperature
	ϵ min	ϵ max		$\tan \delta$	porosity				
Mesosiderite	12.3	–	8	3×10^{-3}	0.3	20–1000	Heggy et al. 2012	RKP A79015	233 K
H5 chondrite	8.6	21.4	5.7	2×10^{-2}	0.3	20–1000	Heggy et al. 2012	LEW 85320	233 K
L5 chondrite	8.4	20.2	5.6	4×10^{-3}	0.3	20–1000	Heggy et al. 2012	MET 01260	233 K
LL5 chondrite	6.9	12.2	4.7	4×10^{-3}	0.3	20–1000	Heggy et al. 2012	MAC 88122	233 K
CM	4.0	4.7	2.9		0.3	20–1000	Kofman et al. 2015	NWA 5797	233 K
CR2	3.5	4.0	2.6		0.3	20–1000	Kofman et al. 2015	NWA 801	233 K
H5	16.0	–	16–33	0.11	solid	450	Campbell 1969	Forest City	Ambient T.
L6	10.6	–	10.6–11.8	5×10^{-2}	solid	450	Campbell 1969	Colby	Ambient T.
L6	9	–	9.0–11.9	4×10^{-2}	solid	450	Campbell 1969	Burderheim	Ambient T.
L6	7.8	–	7.8	1.5×10^{-2}	solid	450	Campbell 1969	Holbrook	Ambient T.

Table 6. Refractory inclusions, chondrules, matrix and metal modal abundances of the some chondrite groups (data from Brearley and Jones, 1998) and corresponding grain density (without porosity, data from Britt et al. 2003). Abundance sums of less than 100 vol% are due to the significant abundance of sulfides.

Chondrite group	CAI	Chondrules (Vol. %)	Matrix (vol. %)	Metal (vol. %)	Density (kg m ⁻³)
CR	0,5	50–60	30–50	5–8	3230 ± 280
CM	5	20	70	0,1	2710 ± 110
H	<0,1	60–80	10–15	8,4	3640 ± 120
L	<0,1	60–80	10–15	4,1	3510 ± 110
LL	<0,1	60–80	10–15	2,0	3480 ± 80

themselves subdivided into groups based on several criteria such as oxygen isotopes, bulk chemical compositions and mineralogy. Among ordinary chondrites, H, L, LL groups are distinguished mostly based on the bulk iron abundance. H chondrites have high total iron contents, L chondrites have low total iron contents and LL chondrites have low metallic iron relative to total iron, as well as low total iron contents (Table 6). CR and CM chondrites are two out of eight groups of carbonaceous chondrites. The average diameter and the abundance of chondrules are some of the parameters used to distinguish them petrographically (Table 6). Chondrites consist of four major component: chondrules, FeNi-metal, refractory inclusions and fine-grained matrix material. The relative abundances of these components vary from one chondrite group to another (Table 6). Calcium-aluminum-rich inclusions (CAIs) are made of corundum, hibonite, grossite, perovskite, melilite, spinel, Al–Ti–diopside, anorthite and forsterite; chondrules are mainly composed of olivine and low-calcium pyroxene crystals with variable FeNi metal grains, set in a feldspathic glass or microcrystalline matrix, the mineralogy of which will depend mostly on the post-accretion processes experienced. Minerals found in matrices include silicates, oxides, sulphides, metallic Fe,Ni and, especially in type 2 chondrites, phyllosilicates and carbonates.

The number commonly attached to the chondrite group (e.g. L5, CR2, ...) provides a guide to the post-accretion history (aqueous alteration and thermal metamorphism) experienced by the chondrites (Van Schmus & Wood 1967). A petrologic type 2 (CR, CM) corresponds to unequilibrated chondrites having mostly escaped thermal metamorphism but having experienced aqueous alteration. Types 5 and 6 designate equilibrated chondrites having experienced significant thermal metamorphism, leading to chemical equilibrium and textural recrystallization.

CM chondrites are characterized by the presence of abundant but relatively small (300 μ m in diameter) chondrules of various chemical compositions (largely FeO-poor type). Due to extensive aqueous

alteration, they are partially replaced by phyllosilicates and FeNi metal is mostly absent. Refractory inclusions are common and fine-grained matrix is highly abundant. The matrix in CM chondrites is mostly composed of phyllosilicates, tochilinite, carbonates, sulphides and magnetite.

In comparison with CMs, CR chondrites are characterized by the presence of abundant large FeNi-metal-rich, porphyritic, magnesian forsterite-rich or enstatite-rich chondrules. Having experienced aqueous alteration but mostly escaped thermal metamorphism, they are also characterized by the presence of an abundant heavily hydrated matrix, where FeNi metal is nevertheless relatively well preserved. Refractory inclusions are much less abundant (Table 6). The hydrated matrix of CR chondrites contains abundant phyllosilicates, carbonates, platelet and framboidal magnetite and sulphides (Weisberg et al. 1993).

Ordinary chondrites are characterized, among other things, by a high abundance of FeO-rich chondrules and rarity of refractory inclusions. They have experienced a large range of thermal metamorphism and type 5 and 6 are nearly equilibrated. The fine-grained matrix has been recrystallized and mineralogy resulting from a hydration event (phyllosilicates, carbonates, ...) is absent, as well as the carbonaceous material present in more primitive chondrites.

Mesosiderites are achondrites that are breccias composed of approximately equal proportions of silicates and Fe,Ni metal plus troilite. Fe,Ni metal is mostly in the form of millimetre or submillimetre grains that are intimately mixed with similarly sized silicate grains such as orthopyroxene, olivine and plagioclase.

Table 5 summarizes the permittivity of meteoritic materials, including measurements performed within the frame of the CONSERT/Rosetta team (Heggy et al. 2012; Kofman et al. 2015). These measurements were carried out on small pellets of powdered material with a porosity estimated as ~30 per cent and the porosity-compensated permittivities give mainly a lower limit. The measurements from Campbell & Ulrichs (1969) are not provided

with estimates of porosity and hence correspond to a lower limit, underestimated if there is any significant porosity. This table confirms the results of Kofman et al. (2015), as, among meteoritic material, only CR2 and CM candidates are consistent with the observed permittivities of the comet (in bold in Table 5).

Nevertheless, a large fraction of the meteorites present in our collections have been found in cold (e.g. Antarctica) or hot (e.g. North West Africa) deserts. They may have experienced various intensities of terrestrial weathering that could result in some rusting and oxidation, among other effects (Bland et al. 2006). This could potentially modify the permittivity values of the bulk meteorite. In particular, the CR2 chondrite NWA 801 is described as having experienced moderate to extensive terrestrial weathering, with pervasive veins of rust occurring throughout (Connolly et al. 2007). On the other hand, the CM chondrite NWA 5797 is not described as terrestrially weathered (Weisberg et al. 2010). Additional laboratory measurements would be required to assess the effect of terrestrial weathering on permittivity precisely. This is outside the scope of the present article, but one can easily foresee that oxidation of the metal fraction will bias the permittivity, inducing a significant underestimation of the actual value for considered CR chondrites in comparison with CM chondrites.

4.2 Mineral materials

A compilation of mineral permittivity available in the literature is presented in Table A1. This set of measurements presents large variability for a given material, due to the variability of the experimental conditions and sample preparation, as mentioned above. In particular, there is a strong variability observed for clay mineral, which can be explained by a variation in sample moisture. In addition, sample alteration including oxidation can also impact the measured permittivity. Caution is advised for laboratory measurements collected at 60 Hz (Rosenholtz 1936). Hence, the value of permittivity derived with CONCERT is at 90 MHz. Confronting this 90 MHz permittivity estimate with measurements at a much lower frequency of 60 Hz is very hazardous.

Most of the measurements have been carried out for a given frequency at near-ambient temperature and one cannot calculate the permittivity at low temperature from the existing measurement: one can simply expect a lower permittivity at lower temperature. The dielectric dependence of materials on temperature is a function of the polarization mechanism and the potential occurrence of dielectric relaxations in the frequency range considered (Parkhomenko 1967). For silicate-rich material in the 90-MHz frequency range considered in this study, there are no observed relaxations that have been observed in a wide variety of geological material (Howell & Licastro 1961). Dielectric measurements of several minerals as a function of temperature in the feldspar group and quartz suggest that, below room temperatures, there is no dielectric dependence of silicate-rich material (Parkhomenko 1967). At 12 kHz, i.e. a frequency significantly below 90 MHz, laboratory measurements have shown that the permittivity of porous dunit decreases from 4.1 to 3.8 when the temperature decreases from 300 K to 80 K (kaolinite 4.4–4.1; montmorillonite 5.15–4.5). We can hence assume that variability of the dust component permittivity is limited in the range of the room temperature to the temperature inside the nucleus.

The confrontation of the literature survey with the permittivity limit derived previously leads to the selection of only a few minerals as clays (illite, kaolinite, montmorillonite), quartz and silica glass (in bold, Table A1). For the dunite (olivine-dominated rock) and

plagioclase feldspar, the porosity of the samples is large but known and the porosity-corrected permittivity can be estimated as values larger than 5.6.

Amorphous silicates are expected to be a major component of cometary and protoplanetary dust. Thermal infrared measurements suggest a mixture of amorphous and crystalline mafic silicates (Wooden 2008). Crystalline Mg-rich silicates (olivine, pyroxenes) and amorphous silicates have been unambiguously detected in protoplanetary discs, in particular in the outer region, where comets are expected to form (Olofsson et al. 2009). Their presence as pure components of 67P/CG dust is ruled out, due to their large permittivity (≥ 6.8 , lab temperature), however they could be mixed up with low-permittivity materials. Silica has been observed in protoplanetary discs and within dust grains from comet Wild 2 (Roskosz & Leroux 2015). Still, SiO₂ (either in crystalline or amorphous form) is expected to be a minor constituent (<10 per cent) according to available observations and laboratory analysis of cometary grains. Finally, plagioclase is the most abundant phase at the surface of the Moon and is a major phase in the crust of differentiated bodies. However, this phase is a minor constituent (<10 per cent) in chondritic meteorites and has never been described as a major constituent of cometary dust from available observations.

As shown in Table A1, clay minerals could have permittivity values below the 5.4 threshold defined above and cannot be excluded based on a literature survey. Phyllosilicates (including clay minerals) are a major constituent of the most primitive meteorites (Brearley 2006). However, these phases are in that case related to an aqueous alteration process that occurred on the parent body. Phyllosilicates have been tentatively identified in the Deep Impact ejecta from 9P/Tempel 1 (8 per cent: Lisse et al. 2006), while hints of the presence of phyllosilicate have been described in *Stardust* grains based on the valence state of iron (Stodolna et al. 2013). In the case of 67P/CG, the measurement for the first time of the reflectance spectra of a comet up to 5 μm permits us to rule out the presence of a significant amount of phyllosilicates in the dust crust (Capaccioni et al. 2015; Quirico et al. 2016), from the lack of absorption centred around 2.7–2.9 μm typically seen in phyllosilicates and hydrated carbonaceous chondrites (Beck et al. 2010). To conclude the survey of dielectric properties of the mineral constituents expected to occur in comets, none of them seems able to explain the value of permittivity of the cometary dust if not mixed with a material with low permittivity.

4.3 Organic materials

Two main groups of organic materials are present in 67P/CG. The first includes so-called refractory organic matter (ROM), which comprises polyaromatic organic solids. Its presence is inferred from the analysis of cometary grains analysed in the laboratory and accounts for the low surface albedo in the visible range. The best optical and chemical analogues of these compounds are terrestrial coals and bitumens (see Quirico et al. 2016 for a detailed discussion). Permittivity measurements on a comprehensive series of coals, covering a broad range of maturity and elemental compositions H/C and O/C, reveal a restricted range of variations of the real part of the permittivity in low-maturity coals (Forniés-Marquina et al. 2003), which are the most relevant analogues of cometary ROM due to their structurally disordered polyaromatic structure.

Forniés-Marquina et al. (2003) show that their permittivity lies between 2 and 3 (Table A2). Very mature coals present a very large permittivity; however, these samples have experienced extensive long-duration thermal metamorphism and are not

Table 7. The different cosmochemical models tested in this study: models 7–9 are consistent with CONSERT measurement and density constraints. Abundances in the third column are given in vol%.

		ϵ min	ϵ max	Density kg m ⁻³	
1	Pure Mg-silicate	7.1	7.9	3200 ± 200	65% olivine 35% pyroxene
2	Ordinary chondrite	6.9	8.4	3510 ± 110	L5–LL5
3	IDP-like	5.3	7.4	2985 ± 265	80% ordinary ch. 20% carbon
4	close to IDPs	5.0	6.4	2922 ± 260	75% ordinary ch. 25% carbon
5	CM carbonaceous chondrite	4.0	4.7	2710 ± 110	CM
6	Mg-silicate and carbon	3.6	4.5	2600 ± 200	33% olivine 17% pyroxene, 50% carbon
7	CR2 carbonaceous chondrite	3.5	4.0	3230 ± 280	CR2
8	Carbon with Mg-silicate	2.6	3.1	2300 ± 200	16% olivine 9% pyroxene, 75% carbon
9	Pure refractory carbon UCAMM-like	2.0	4.0	2000 ± 200	100% carbon

relevant analogues for cometary ROM. The effects of ash contents and moisture have been found to be weak or negligible; therefore these measurements can be extrapolated to pure organic materials in vacuum conditions. The sample porosity is not measured in the study of Forniés-Marquina et al. (2003) and leads them to underestimate the dielectric permittivity. All the measurements were done at ambient temperature, most probably meaning that permittivity is lower for the low temperatures inside the comet. As previously explained, we will keep in mind this fact in our conclusions.

Hotta et al. (2011) report permittivity measurements on another series of coals for which a relative density could be determined (the relative density is the ratio of the apparent density to the material density). Extrapolation of these measurements (see fig. 7 in Hotta et al. 2011) provides a real part of the permittivity value between 3 and 4 at 10 GHz, which corresponds to the range given by the HS lower limit calculations (3.2–3.8).

The bitumen shows lower permittivities 2.5–2.7 (Table A2; von Hippel 1954; Green 1977) in our frequency range at ambient temperature. These values would also probably be lower for low temperatures inside the nucleus.

The second group of organic materials comprises a broad diversity of so-called semi-volatile molecules, ions or even polymers like polyoxymethylene (Capaccioni et al. 2015; Goesmann et al. 2015; Wright et al. 2015). The broad 3.2- μ m band detected by the VIRTIS imaging spectrometer may point to the large abundance of carboxylic acids, which also constitute the dominant molecular species in the so-called soluble organic matter (SOM) extracted from primitive meteorites (Sephton et al. 2003; Schmitt-Kopplin et al. 2010). Only a few permittivity measurements are available for the species that constitute the SOM fraction or species that are presumably present as ions or polymers. However, some trends can be inferred regarding data catalogues usually issued for industrial applications (Von Hippel 1954).

Table A2 compiles some permittivities of liquid materials having some relevance or similarities with what is expected for the 67/CG comet. The permittivity of ethyl alcohol decreases from $\epsilon = 23$ at frequencies lower than 300 MHz to $\epsilon = 1.7$ at 10 GHz (Table A2 and von Hippel section II.1). Given the similarities with the behaviour of liquid water ($\epsilon = 80$ in the MHz band) and ice ($\epsilon = 3.2$ in the MHz band, while the static permittivity is $\epsilon = 80$), we can expect a permittivity of solid ethyl alcohol close to $\epsilon = 1.7$. Similar behaviours can be noted for some other alcohols, even if the permittivity was measured up to 10 GHz only, a frequency lower than the relaxation frequency and not allowing estimation of ϵ_∞ .

Screening the catalogue of Von Hippel (1954) reveals that most organic solids with some similarities with the expected material (Table A2) have a permittivity in the 2.0–3.3 range.

It may thus be concluded from this study that the permittivity of the organic material present in the bulk of the comet (including both refractory and semi-volatile fractions) ranges from 2–4.

4.4 Cosmochemical models

In order to assess further the implications of the permittivity measurements obtained with CONSERT, different cosmochemical models were defined and their permittivity was computed (Table 7). These models were designed to test different scenarios, given present-day knowledge of the small bodies population.

First, extraterrestrial materials with measured permittivity were used. In that line, ordinary chondrites were used (the most abundant meteorite type falling on Earth: Table 7, line 2) as well as carbonaceous chondrites CM and CR2 (Table 7, lines 5 and 7). The latter were chosen since the relation between carbonaceous chondrites and comets has been discussed (Gounelle, Spurný & Bland 2006). In particular, CR chondrites were used, a family for which affinities with cometary material as sampled by the *Stardust* mission has been discussed. In addition, the infrared spectra of some CR chondrites in the 10- μ m region can be similar to observations of cometary dust (Beck et al. 2014).

In parallel, model material mixtures were computed whenever dielectric measurements were absent for appropriate analogues. To begin with, a pure silicate model was built in order to model cometary dust devoid of any metal and sulphides (unlike the case of ordinary chondrites). A mixture with 65 per cent olivine + 35 per cent pyroxene was tested, which is in rough agreement with the estimated composition of the outer regions of accretion discs (Pollack et al. 1994; see also Table 7, line 1).

In addition, several models were built in order to mimic the composition of interplanetary dust particles collected in the stratosphere (IDPs). First, we used a silicate and carbon mixture with mixing ratio 80 per cent–20 per cent and 75 per cent–25 per cent, in order to represent standard chondritic porous IDPs (Table 7, lines 3 and 4). In addition, a carbon-pure model was defined in order to represent the equivalent of the so-called ultra-carbonaceous Antarctic micrometeorites (UCAMMs: Table 7, line 9). This recently identified micrometeorite type is basically dominated by macromolecular organic matter (Dartois et al. 2013). Finally, models in between standard IDPs and UCAMM were built, with silicate–carbon mixing ratios of 50 per cent–50 per cent and 25 per cent–75 per cent (Table 7, lines 6 and 8).

Among the models developed, several can be classified as inconsistent with 67P/CG observations based solely on the calculated value of permittivity. These are the pure silicate and ordinary chondrites, for which calculated values of permittivities are higher than 6.9 (Table 7, lines 1–2).

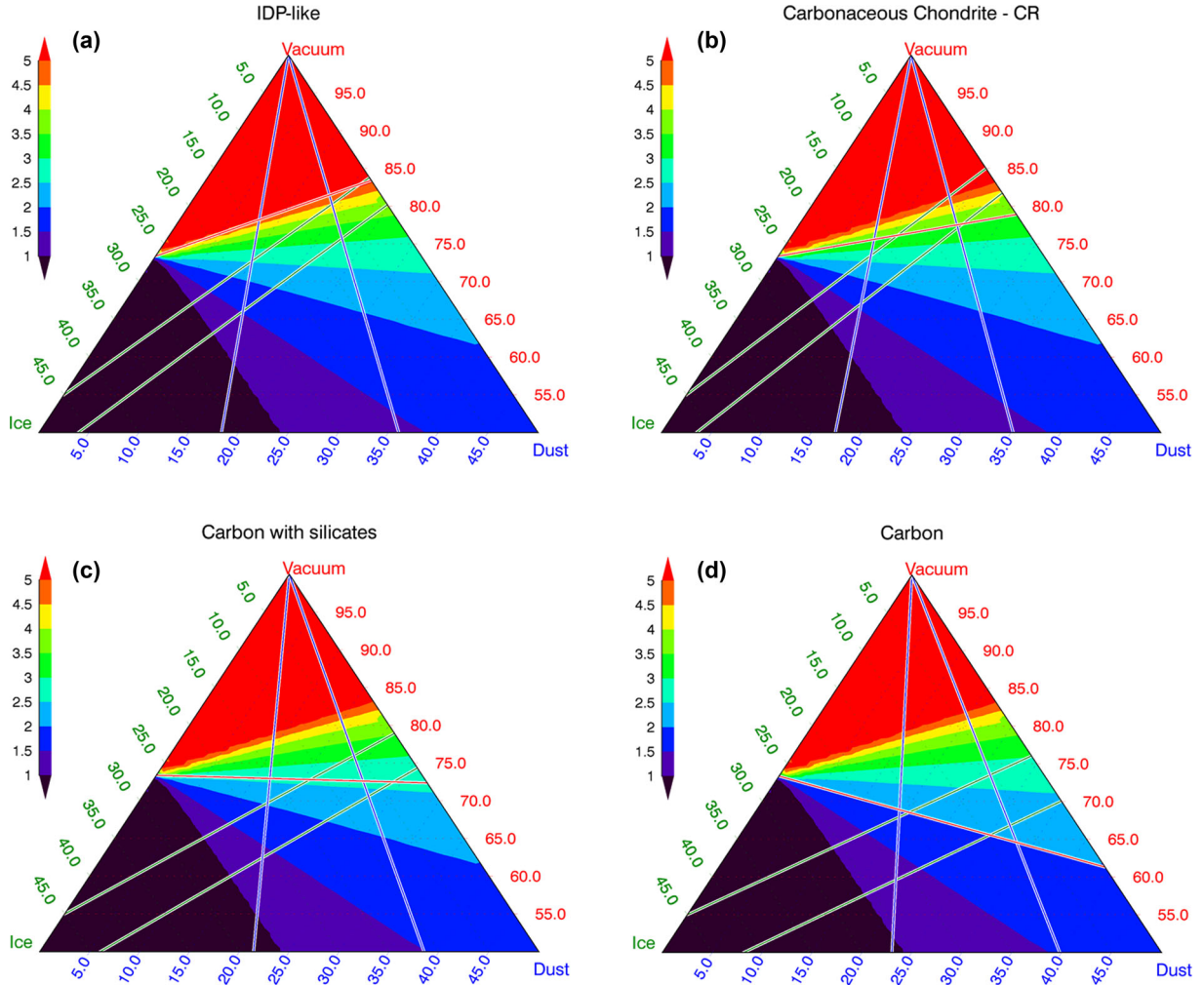


Figure 5. Updated ternary diagram with the relevant density for cosmochemical models.

This is also the case for the IDP-like composition with permittivity equal to 5.3 (Table 7, line 3). This value corresponds to the red line in Fig. 5(a) and the entire domain above this line is compliant with CONSERT measurements. However, for this material, the density of the mixture is estimated to be around 3000 kg m^{-3} (in practice we consider $\pm 200 \text{ kg m}^{-3}$ margins). Using such density values, the dust permittivity upper limit is no longer equal to 5 but decreases to 4.4. As a consequence, this model has to be rejected from density considerations and the same for the IDP-like composition with a little more organics (25 per cent instead of 20 per cent: Table 7, line 4).

A similar approach can be applied to the CM carbonaceous chondrite models (Table 7, line 5). The possible domain defined by density and D/I corresponds to a permittivity lower than 3.5, which is lower than the calculated permittivity of the mixture. CM carbonaceous chondrites are rejected by their density. It is the same for a 50 per cent Mg-silicate and carbon mixture (Table 7, line 7).

The CR carbonaceous chondrite model could explain CONSERT measurements (Table 7, line 6): its density of around 3230 kg m^{-3} induces porosity larger than 75 per cent and is compliant with a permittivity equal to 3.5 (Fig. 5b). However, CR2 chondrites can be ruled out because their composition is inconsistent with the lack of hydrated minerals in 67P/C, as revealed by the VIRTIS instrument. Outside the CR2 meteoritic material, the only models that are able

to respect both the permittivity and density constraint successfully are those containing a high amount of organic compounds (≥ 75 per cent).

In other words, the dielectric measurements obtained by CONSERT imply that a major fraction of the dust has a low dielectric permittivity and the permittivity limit depends on the dust density. This constraint is plotted in Fig. 6: for a given dust density, its permittivity has to be equal to or lower than the plotted limit to be compliant with CONSERT measurements. If the permittivity is close to the limit, there is only one possible D/I ratio, which corresponds to a maximum of porosity (point B in Fig. 1 for the corresponding dust density): the corresponding dust and ice ratios are the ones plotted in Fig. 6.

A lower porosity necessarily leads to a dust fraction with a lower permittivity (we move away from point B in the ternary diagram in Fig. 1). Conversely, a dust permittivity lower than the limiting value does not necessarily imply a lower porosity. This difference may in fact be due to uncertainties in the dielectric model, the permittivity of the ice fraction and the CONSERT measurements, as discussed in section 3 and Fig. 4.

This low permittivity of the dust fraction clearly excludes silicate-rich candidates. The prime candidate then seems organics, this result needing to be consolidated with laboratory measurements under controlled conditions of temperature and porosity and a relevant frequency range.

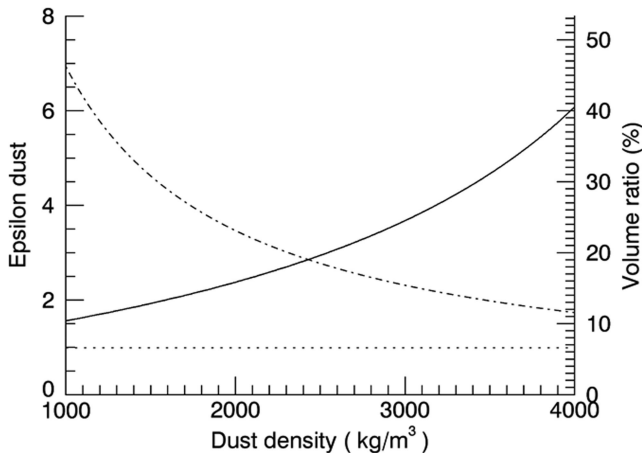


Figure 6. Maximum dust permittivity as a function of the dust density (continuous line and left axis) and the corresponding dust (dashed line) and ice (dotted line) volume fraction (right axis). Values correspond to the upper corner of the domain of interest for this density (point B in Fig. 1).

4.5 Cosmochemical implications

The results obtained in the present study suggest that the dust particles from Comet 67P/CG are on average carbon-rich (>75 vol. per cent) and could provide insights on the origin of cometary organics and the relation between cometary grains and other types of cosmomaterials.

The Solar system value for the carbon-to-silicon ratio can be inferred from measurements of the solar photosphere (Lodders 2010). The C/Si value of the Sun is 7.2, well above the value measured for one of the most C-rich carbonaceous chondrites, Orgueil (C/Si = 0.77: Lodders 2010). The atomic C/Si ratio of the different cosmochemical models (Table 7) can be estimated by supposing that the silicates are Mg-rich (with a density of 3.4) and that the organics are in a pure carbon form (with a density of 2). The C/Si values that are found are 1.4 for the IDP model, 1.9 for model 4 (close to IDP), 5.7 for model 6 (50 silicates/50 carbon) and 17.0 for model 7 (25 silicate/75 carbon). As cosmochemical models from 6–8 match CONSERT observations, the suggestion is made that cometary grains have a C/Si ratio of at least 5.7. Such a high value was previously estimated for dust particles from comet Halley (C/Si = 5.8: Jessberger, Christoforidis & Kissel 1988). This is at least twice the value of the CI chondrite and probably more than the average IDPs. This difference suggests that the CI chondrite Orgueil and comets are from different initial reservoirs (which is unexpected given the similarity between the Solar composition and Orgueil for heavy elements) or that at some stage carbon was lost in the case of the CI chondrite. The only known extraterrestrial materials available in the laboratory that match CONSERT observations are the UCAMMs, a peculiar type of carbon-rich micrometeorite (Dartois et al. 2013). In contrast, chondritic porous interplanetary dust particles typically have a carbon content between 4 and 45 per cent by weight (estimated C/Si 0.45–4.85), with an average value around 13 per cent by weight (C/Si = 1.4: Keller, Thomas & McKay 1994; Bradley 2007). However, UCAMMs are very scarce and are certainly not representative of the majority of comets. Moreover, they also may not be representative of the interior of a cometary nucleus, as their nitrogen abundance is best accounted for by formation in the uppermost region of the surface (Dartois et al. 2013).

An alternate explanation is that cosmomaterials available in the laboratory only account for the most refractory organic materials.

Another component, described as semi-volatile organics, may be present in the cold nucleus and at the surface of 67P/CG. By semi-volatile, we mean less volatile than ices, but with more volatiles than organics found in carbonaceous chondrites and IDPs. This component would not be stable enough to survive a long residence in the interplanetary medium and might account for the high carbon ratio provided by CONSERT data. This result would tend to fit with observations by VIRTIS (Quirico et al. 2016), COSAC (Goesmann et al. 2015) and Ptolemy (Wright et al. 2015), who propose that some amount of organics is present in a condensed *semi-volatile* form and could for instance be detected by mass spectrometers in sniffing modes.

In conclusion, the sounding of the 67P/CG nucleus with the CONSERT bistatic radar outlines the presence of an abundant organic component, the most volatile fraction of which is not sampled by meteorites and interplanetary dust.

5. CONCLUSION

On 67P/CG, CONSERT measured an averaged permittivity equal to 1.27 ± 0.05 , which implies that the dust permittivity is lower than 5.4 according to the tested mixing formula. This value is an upper limit, corresponding to dust without any micro or macro porosity, for a dust-to-ice ratio equal to 4 ± 2 , a nucleus bulk density equal to $533 \pm 6 \text{ kg m}^{-3}$ and a dust density ranging from $2000\text{--}3500 \text{ kg m}^{-3}$.

The compliance with the CONSERT measurement dust permittivity limit varies significantly with the assumed dust density (Fig. 6): a decrease of dust density induces an increase of its volume fraction (to match the nucleus density) and then implies a lower dust permittivity. Analysis of the cosmochemical implications of the CONSERT permittivity measurement requires us to take into account both material density and permittivity (Fig. 6): neither minerals nor meteoritic samples as known from the literature can explain the CONSERT value, except for CR2. However, CR2 chondrites can be ruled out, because their composition is inconsistent with the lack of hydrated minerals in 67P/C, as revealed by the VIRTIS instrument. Based on the same approach, tholins as studied by Brouet et al. (2016) can be excluded, since they are characterized by a low density associated with a relatively high permittivity ($\epsilon = 1.6$ for 75 per cent porosity). Note also that the high nitrogen content of those tholins is not consistent with the composition of the surface of 67P/CG.

Several composition models were tested, in order to span the different cosmochemical models of cometary dust. They include pure silicate dust and its mixture with increasing content of a carbonaceous material (comprising both insoluble and soluble species). These calculations show that an important fraction of carbonaceous material is required in the dust in order to match CONSERT permittivity observations. The minimum required content of the carbonaceous material is 75 vol. per cent, which is about 2.5 times higher than the CI chondrite Orgueil and more carbon-rich than typical interplanetary dust particles. This is in agreement with previous *in situ* measurements of cometary dust and suggests that comets represent a massive carbon reservoir. Finally, these results also demonstrate the lack of connection between carbonaceous chondrites and 67P/CG and confirm that Antarctic micrometeorites and stratospheric IDPs are cometary material available in the laboratory.

Today, the permittivity values of extraterrestrial materials available in the literature are rather scarce and mostly measured on metamorphosed ordinary chondrites. These meteorites cannot be considered as model material of cometary samples.

Our interpretation presented in this article is based on present knowledge of the dielectric properties of materials and their dependence on frequency and temperature. This knowledge is certainly limited, especially for possible types of cometary dust and ices. In that sense, our conclusions only provide indications on the possible composition of the cometary interior.

To be able to consolidate this analysis and interpret the CONSERT data further, additional laboratory measurements on samples that are more relevant to comets (in terms of mineralogy and carbonaceous material composition) are required. Ideally, one would want to perform these measurements on IDPs and micrometeorites of potential cometary origin, but, due to their small size, this would represent a real analytical achievement. Complementary measurements on synthesized organic molecules (refractory and semi-volatiles) and defined mixtures of minerals and organic molecules should also be envisaged.

ACKNOWLEDGEMENTS

Support from the Centre National d'Etudes Spatiales (CNES, France) for this work, based on observations with CONSERT on board *Rosetta*, is acknowledged. The CONSERT instrument was designed built and operated by IPAG, LATMOS and MPS and was financially supported by CNES, CNRS, UGA, DLR and MPS. *Rosetta* is an ESA mission with contributions from its Member States and NASA. *Rosetta*'s Philae lander is provided by a consortium led by DLR, MPS, CNES and ASI. The authors thank the teams of *Rosetta* (SGS and ESOC) and Philae (LCC and SONC) for making the CONSERT operations possible.

REFERENCES

A'Hearn M. F., Millis R. C., Schleicher D. O., Osip D. J., Birch P. V., 1995, *Icarus*, 118, 223
 Andersson O., 2008, *J. Phys. Condensed Matter*, 20, 244115
 Beck P. et al., 2010, *Geochimica et Cosmochimica Acta*, 74, 4881
 Beck P., Garenne A., Quirico E., Bonal L., Montes-Hernandez G., Moynier F., Schmitt B., 2014, *Icarus*, 229, 263
 Biele J. et al., 2015, *Science*, 349, aaa9816
 Bieler A. et al., 2015, *Nature*, 526, 678
 Bland P. A., Zolensky M. E., Benedix G. K., Sephton M. A., 2006, in Lauretta D. S., McSween H. A., eds, *Meteorites and the Early Solar System II*. University of Arizona Press, Tucson, p. 853
 Bockelée-Morvan D., 2015, *A&A*, 583, A6
 Bradley J. P., 2007, in Turekian K. K., ed., *Treatise on Geochemistry*. Pergamon, Oxford, p. 1
 Brearley A. J., 2006, in Lauretta D. S., McSween H. A., eds, *Meteorites and the Early Solar System II*. University of Arizona Press, Tucson, p. 587
 Britt D. T., Consolmagno G. J., 2003, *Meteoritics Planet. Sci.*, 38, 8
 Brouet Y. et al., 2016, *MNRAS*, in press
 Brownlee D., Joswiak D., Matrajt G., 2012, *Meteoritics Planet. Sci.*, 47, 453
 Campbell M. J., Ulrichs J., 1969, *J. Geophys. Res.*, 74, 5867
 Capaccioni F. et al., 2015, *Science*, 347, aaa0628
 Chow R. S., Tse D. L., Takamura K., 2004, *Canada J. Chem. Eng.*, 82, 840
 Cochran A. et al., 2015, *Space Sci. Rev.*, 197, 9
 Connolly H., Smith C., Benedix G., Folco L., Righter K., Zipfel J., Yamaguchi A., Chennaoui Aoudjehane H., 2007, *Meteoritics Planet. Sci.*, 42, 1647
 Consolmagno G. J., Britt D. T., Macke R. J., 2008, *Chemie der Erde*, 68, 1
 Consolmagno G. J., Schaefer M. W., Schaefer B. E., Britt D. T., Macke R. J., Nolan M. C., Howell E. S., 2013, *Planet. Space Sci.*, 87, 146
 Daniels D. J., ed., 1996, *Surface-Penetrating Radar*. The Institution of Electrical Engineers Press, London
 Dartois E. et al., 2013, *Icarus*, 224, 243
 Davidsson B. J. R., Gutiérrez P. J., 2005, *Icarus*, 176, 453

Davis J. L., Annan A. P., 1989, *Geophysical Prospecting*, 37, 531
 De Sanctis M. C., Lasue J., Capria M. T., Magni G., Turrini D., Coradini A., 2010, *Icarus*, 207, 341
 Ehrenfreund P., Charnley S. B., 2000, *ARA&A*, 38, 427
 Festou M. C., Keller H. U., Weaver H. A., 2004, in Festou M. C., Keller H. U., Weaver H. A., eds, *Comets II*. University of Arizona Press, Tucson, p. 3
 Forniés-Marquina J. M., Martín J. C., Martínez J. P., Miranda J. L., Romero C., 2003, *Canadian J. Phys.*, 81, 599
 Fulle M., Barbieri C., Cremonese G., Rauer H., Weiler M., Milani G., Ligustri R., 2004, *A&A*, 422, 357
 Goesmann F. et al., 2015, *Science*, 349, aab0689
 Gough S. R., 1972, *Can. J. Chem.*, 50, 3046
 Gounelle M., Spurný P., Bland P. A., 2006, *Meteoritics Planet. Sci.*, 41, 135
 Green E. H., 1977, *An Acceptance Test for Bitumen for Rolled-Asphalt Wearing Course*. Transport and Road Research Laboratory, Crowthorne.
 Gulkis S. et al., 2015, *Science*, 347, aaa0709
 Hahnel R., Hegler S., Stätz C., Plettemeier D., Zine S., Herique A., Kofman W., 2015, *Planet. Space Sci.*, 111, 15
 Hanner M. S. et al., 1985, *Icarus*, 64, 11
 Hässig M. et al., 2015, *Science*, 347, aaa0276
 Heggy E., Palmer E. M., Kofman W., Clifford S. M., Righter K., Herique A., 2012, *Icarus*, 221, 925
 Herique A., Kofman W., Hagfors T., Caudal G., Ayanides J. P., 1999, *Planet. Space Sci.*, 47, 885
 Herique A., Gilchrist J., Kofman W., Klinger J., 2002, *Planet. Space Sci.*, 50, 857
 Herique A., Rogez Y., Pasquero O. P., Zine S., Puget P., Kofman W., 2015, *Planet. Space Sci.*, 117, 475
 Hoang M. et al., 2017, *A&A*, in press
 Hotta M., Hayashi M., Lanagan M. T., Agrawal D. K., Nagata K., 2011, *ISIJ Int.*, 51, 1766
 Howell B. F., Licastro P. H., 1961, *American Mineralogist*, 46
 Jessberger E., Christoforidis A., Kissel J., 1988, *Nature*, 332, 691
 Jones R. G., 1976, *J. Phys. D: Applied Phys.*, 9, 819
 Kamoun P., Lamy P. L., Toth I., Herique A., 2014, *A&A*, 568, A21
 Keller L. P., Thomas K. L., McKay D. S., 1994, *Meteoritics*, 29, 480
 Kelley M. S., Wooden D. H., Tubiana C., Hoenhardt H., Woodward C. E., Harker D. E., 2009, *AJ*, 137, 4633
 Kelley M. S., Wooden D. H., 2009, *Planet. Space Sci.*, 57, 1133
 Kissel J. et al., 1986, *Nature*, 321, 280
 Klinger J. et al., 1996, *Planet. Space Sci.*, 44, 637
 Kofman W. et al., 1998, *Adv. Space Res.*, 21, 1589
 Kofman W. et al., 2007, *Space Sci. Rev.*, 128, 413
 Kofman W. et al., 2015, *Science*, 349, aaa0639
 Krishna Swamy K. S., 1991, *A&A*, 241, 260
 Lamy P. et al., 2007, *A&A*, 458, 669
 Lasue J., De Sanctis M. C., Coradini A., Magni G., Capria M. T., Turrini D., Levasseur-Regourd A. C., 2008, *Planet. Space Sci.*, 56, 1977
 Le Roy L. et al., 2015, *A&A*, 583, A1
 Lethuillier A. et al., 2016, *A&A*, 591, A32
 Levasseur-Regourd A. C., Zolensky M., Lasue J., 2008, *Planet. Space Sci.*, 56, 1719
 Levasseur-Regourd A. C., Hadamcik E., Desvoivres E., Lasue J., 2009, *Planet. Space Sci.*, 57, 221
 Li A., Greenberg J. M., 1997, *A&A*, 323, 566
 Lide D. R., ed., 2005, *CRC Handbook of Chemistry and Physics*, 86th edn. CRC Press, Boca Raton, FL
 Lisse C. M. et al., 2006, *Science*, 313, 635
 Lodders K., 2010, in Goswami A., Reddy B. E., eds, *Principles and Perspectives in Cosmochemistry*. Astrophysics and Space Science Proceedings, Springer-Verlag, Berlin, p. 379
 Marboeuf U., Schmitt B., 2014, *Icarus*, 242, 225
 Martinez A., Byrnes A. P., 2001, *Current Res. Earth Sci.: Kansas Geological Survey*, 247, 1
 Morse A., Mousis O., Sheridan S., Morgan G., Andrews D., Barber S., Wright I., 2015, *A&A*, 583, A42
 Mumma M. J., Charnley S. B., 2011, *A&A*, 49, 471

- Olhoeft G. R., 1979, Electrical Properties of Rocks: tables of room temperature electrical properties for selected rocks and minerals with dielectric permittivity statistics, USGS report 79-993
- Olofsson J. et al., 2009, A&A, 507, 327
- Parkhomenko E. I., 1967, Electrical Properties of Rocks. Plenum Press, New York
- Pätzold M. et al., 2007, Space Sci. Rev., 128, 599
- Pätzold M. et al., 2016, Nature, 530, 63
- Pettinelli E. et al., 2003, J. Geophys. Res., 108, 8029
- Pilla S. et al., 1999, Phy. Lett. A, 256, 24
- Pollack J. B. et al., 1994, ApJ, 421, 615
- Preusker F. et al., 2015, A&A, 583, A33
- Prialnik D. et al., 2004, Comets II, 1, 359
- Quirico E. et al., 2016, Icarus, 272, 32
- Robinson D. A., 2004, Soil Sci. Soc. America J., 68, 1780
- Rosenberg E. D., Prialnik D., 2010, Icarus, 209, 753
- Rosenholtz J. L., Smith D. T., 1936, American Mineralogist, 21, 115
- Roskosz M., Leroux H., 2015, ApJ Lett., 801, L7
- Rotundi A. et al., 2015, Science, 347, aaa3905
- Rubin M. et al., 2015, Science, 348, 232
- Saint-Amant M., Strangway D. W., 1970, Geophysics, 35, 624
- Schmitt-Kopplin P. et al., 2010, Proc. Natl. Acad. Sci., 107, 2763
- Sephton M. A. et al., 2003, Geochim. Cosmochim. Acta, 67, 2093
- Shannon R. D., Subramanian M. A., Hosoya S., Rossman G. R., 1991, Phys. Chemistry Minerals, 18, 1
- Shebani N. M., Khamoudi B. M., Abul-kassem A. S., 2009, 2nd International Conference on Computer and Electrical Engineering. IEEE Computer Society, CA, p. 352
- Sierks H. et al., 2015, Science, 347, aaa1044
- Sihvola A., Lindell IV., 1989, Journal of Electromagnetic Waves and Applications, 3, 37
- Sihvola A., 1999, Electromagnetic Mixing Formulas and Applications. The Institute of Electrical Engineers, London
- Spohn T. et al., 2015, Science, 349, aab0464
- Stillman D., Olhoeft G., 2008, J. Geophys. Res., 113, E09005
- Stodolna J., Gainsforth Z., Leroux H., Butterworth A. L., Tyliszczak T., Jacob D., Westphal A. J., 2013, Geochim. Cosmochim. Acta, 87, 35
- Telford W. M., Geldart L. P., Sheriff R. E., 1990, Applied Geophysics. Cambridge University Press, Cambridge
- von Hippel A., 1954, Dielectric Materials and Application. Chapman & Hall, London
- Van Schmus W. R., Wood J. A., 1967, Geochim. Cosmochim. Acta, 31, 747
- Watanabe N., Kouchi A., 2008, Prog. Surf. Sci., 83, 439
- Weiler M. et al., 2004, A&A, 414, 749
- Weisberg M. K., Prinz M., Clayton R. N., Mayeda T. K., 1993, Geochim. Cosmochim. Acta, 57, 1567
- Weisberg M. K. et al., 2010, Meteoritics Planet. Sci., 45, 449
- Wooden D. H., 2008, Space Sci. Rev., 138, 75
- Wright I. P. et al., 2015, Science, 349, 6247
- Xu H., Vij J. K., McBrierty V. J., 1994, Polymers, 35, 227

APPENDIX

Table A1. Dielectric permittivity of minerals: a compilation from the literature. epsilon: real permittivity; tan delta: loss tangent. Temperature and sample origin are given when known. ‘Extrapolation @ 90 MHz’ denotes an extrapolation of permittivity from low frequency to 90 MHz calculated in Herique et al. (2002). (In bold: minerals compliant with the CONCERT permittivity.)

MINERALS					
ϵ	1000*tan δ	Frequency	Porosity	Note	References
<i>Serpentine (Mg,Fe,Ni)3Si2O5(OH)4</i>					
6.4 (6.4)	40 (11)	35 (450) MHz		Cardiff, Md	Campbell 1969
6.4 (7.0)	60 (19)	35 (450) MHz		Oregon	Campbell 1969
6.6		100 MHz			Telford, Geldart & Sheriff 1990
11.1	116	1 MHz	0	Cardiff, Md	Olhoeft 1979
11.5		60 Hz	(Powder)	$T = 20^\circ\text{C}$	Rosenholtz 1936
14.0		1 MHz	0		Olhoeft 1979
<i>Peridotite changing to serpentine</i>					
7.6 (7.5)	11 (8)	35 (450) MHz		Lowell, Vt	Campbell 1969
<i>Olivine (Mg, Fe)2SiO4</i>					
6.8		60 Hz		$T = 20^\circ\text{C}$	Rosenholtz 1936
7.03 – 7.61	< 1	1 MHz		$0^\circ\text{C} < T < 30^\circ\text{C}$	Shannon et al. 1991
7.1	4.3	1 MHz	0	Washington	Olhoeft 1979
7.2		1 MHz			Martinez 2001
7.3	40	1 MHz	0	Colorado	Olhoeft 1979
<i>Fayalite Fe2SiO4</i>					
6.8		1 MHz	0		Olhoeft 1979
8.58 – 8.92	1	1 MHz		$0^\circ\text{C} < T < 30^\circ\text{C}$	Shannon et al. 1991
<i>Forsterite Mg2SiO4</i>					
6.8		1 MHz	0		Olhoeft 1979
7.6	0.8	1 MHz			Shannon et al. 1991
<i>Dunite</i>					
3.7–4.3		90 MHz	40–55%	Extrapolation @ 90 MHz	Herique et al. 2002
3.8–4.3	0.1–10	0.12–12 kHz	40–55%	78–360 K	Herique et al. 2002
<i>Pyroxenes</i>					
7.9	8	1 MHz	0	Helena, Mt	Olhoeft 1979
8.5		1 MHz			Olhoeft 1979
<i>Enstatite (ortopyroxene) MgSiO3</i>					
8.2		60 Hz	(Powder)	$T = 20^\circ\text{C}$	Rosenholtz 1936

Table A1 – continued

MINERALS					
ε	$1000 \times \tan \delta$	Frequency	Porosity	Note	References
<i>Augite (clinopyroxene) (Ca,Na)(Mg,Fe,Al,Ti)(Si,Al)2O6</i>					
6.7		60 Hz	(Powder)	$T = 20^\circ\text{C}$	Rosenholtz 1936
9.3		1 MHz	0		Olhoeft 1979
<i>Diopside (clinopyroxene) MgCaSi2O6</i>					
7.9	25.6	1 MHz	0	Finland	Olhoeft 1979
8.6		1 MHz	0		Olhoeft 1979
<i>Hedenbergite (clinopyroxene) CaFeSi2O6</i>					
9.0		60 Hz	(Powder)	$T = 20^\circ\text{C}$	Rosenholtz 1936
12.4	183	1 MHz	0		Olhoeft 1979
17.4		1 MHz	0		Olhoeft 1979
<i>Plagioclase feldspar KAlSi3O8–NaAlSi3O8–CaAl2Si2O8</i>					
3,3–3,4		0.1–1 MHz	0.43	(8.1 wo porosity)	Saint-Amant 1970
5.4–7.1		100 MHz			Telford et al. 1990
<i>Anorthite CaAl2Si2O8</i>					
6.9		60 Hz	(Powder)	$T = 20^\circ\text{C}$	Rosenholtz 1936
6.9		1 MHz	0		Olhoeft 1979
<i>Magnetite (spinel group) Fe3O4</i>					
33.7 < < 81		60 Hz	(Powder)	$T = 20^\circ\text{C}$	Rosenholtz 1936
<i>Hematite + magnetite</i>					
15.0	200	50 MHz			Stillman 2008
<i>Spinel MgAl2O4</i>					
6.8		60 Hz	(Powder)	$T = 20^\circ\text{C}$	Rosenholtz 1936
<i>Pyrrhotite Fe(1-x)S (x = 0 to 0.2)</i>					
<81		60 Hz	(Powder)	$T = 20^\circ\text{C}$	Rosenholtz 1936
<i>Calcite CaCO3</i>					
6.4		1 MHz	0		Olhoeft 1979
6.4		60 Hz	(Powder)	$T = 20^\circ\text{C}$	Rosenholtz 1936
6.4		1 MHz		$0^\circ\text{C} < T < 30^\circ\text{C}$	Martinez 2001
7.8–8.5		100 MHz		$0^\circ\text{C} < T < 30^\circ\text{C}$	Telford et al. 1990
9.1	50	0.1 MHz	0	Canada	Olhoeft 1979
9.8	34	10 kHz	0	Canada	Olhoeft 1979
<i>Dolomite CaMg(CO3)2 with traces of Fe; Mn; Co; Pb; Zn</i>					
7.5		1 MHz	0		Olhoeft 1979
7.7	27	1 MHz		Porosity = 0, Thornwood, NY	Olhoeft 1979
<i>Clays</i>					
2.7		2.68 GHz			Shebani, Khamoudi & Abul-kassem 2009
4–6		100 MHz		Dry clay	Daniels 1996
5–40		100 MHz			Davis 1989
10–15		100 MHz		Wet clay	Daniels 1996
<i>Kaolinite Al2(Si2O5)(OH)4</i>					
4.0–4.6		90 MHz	30%	Extrapolation @ 90 MHz	Herique et al. 2002
4.1–6.1	0.3–80	0.12–12 kHz	30%	78–360 K	Herique et al. 2002
4.4–5.8		1–1750 MHz	0		Robinson 2004
11.8		1 MHz	0		Olhoeft 1979
<i>Illite (K,H3O)(Al,Mg,Fe)2(Si,Al)4O10 [(OH)2,(H2O)]</i>					
5.6–6.0		1–1750 MHz	0		Robinson 2004
10.0		1 MHz	0		Olhoeft 1979
<i>Montmorillonite (smectites group) (Na, Ca)0,3(Al, Mg)2Si4O10(OH)2·nH2O</i>					
4.2–4.8		90 MHz	<20%	extrapolation @ 90 MHz	Herique et al. 2002
4.5–7	1–100	0.12–12 kHz	<20%	78–360 K	Herique et al. 2002
5.5		1–1750 MHz	0		Robinson 2004
207.0		1 MHz	0	(erroneous value ?)	Olhoeft 1979
<i>Quartz</i>					
4.4–4.6		1 kHz–35 GHz			Jones 1976
<i>Silica glass</i>					
3.8	0.2	1–100 MHz		$T = 20^\circ\text{C}$	von Hippel 1954

Table A2. Dielectric permittivity of solid organics and carbon (from the literature).

Carbon and organics	ϵ	Frequency	Porosity	Note	References
Carbon					
Diamond	4.58	60 Hz			Rosenholtz 1936
Graphites	15–23	1–10 GHz	28%		Hotta et al. 2011
Artificial graphites	20–30		75%		Hotta et al. 2011
Pure carbon	23–30		36%		Hotta et al. 2011
Carbon black	6.0–9.0		78%		Hotta et al. 2011
COAL					
Coal powder	1.94–2.21	1–10 GHz	~50%		Hotta et al. 2011
Lignites	1.9–2.8	DC- 5 GHz	porous		Forniés-Marquina et al. 2003
Anthracites (H/C > 0.5)	2.0–2.5	DC- 5 GHz	porous		Forniés-Marquina et al. 2003
Anthracites (H/C < 0.25)	4.0–14.8	DC- 5 GHz	porous	very mature	Forniés-Marquina et al. 2003
Subbituminous coal	2.1–3.1	DC- 5 GHz	porous		Forniés-Marquina et al. 2003
Bituminous coal	2.0–2.5	DC- 5 GHz	porous		Forniés-Marquina et al. 2003
Bitumen mixtures of hydrocarbons with high molecular weight					
Bitumens	2.5–2.7	1 kHz–1 GHz			von Hippel 1954
Petroleum bitumen	2.65	1.59 KHz	non-porous		Green 1977
Complex organics – solids					
Paraffin	2–2.25	1–100 MHz		25 °C	von Hippel 1954
Naphtalene	2.8–2.9	10 MHz–1 GHz	(crystal)	25 °C	von Hippel 1954
Orthoterphenyl	2.75–2.8	10 MHz–1 GHz	(crystal)	25 °C	von Hippel 1954
Gilsonite	2.5	10 MHz–1 GHz		25 °C	von Hippel 1954
Waxes	2.0–3.3	10 MHz–1 GHz		25 °C	von Hippel 1954
Complex organics – liquids					
Toluene	2.3	1 kHz	liquid	30 °C	Chow, Tse & Takamura 2004
Hepatne	1.97	10 MHz–300 MHz	liquid		von Hippel 1954
Ethyl alcohol	22–24	10 MHz–300 MHz	liquid		von Hippel 1954
Ethyl alcohol	1.7	10 GHz	liquid		von Hippel 1954
Dioctyl sebacate	2.75–4.0	1 MHz–3 GHz	liquid		von Hippel 1954
n-propyl alcohol	19–20	1 MHz–100 MHz	liquid		von Hippel 1954
n-propyl alcohol	2.3	1 GHz	liquid		von Hippel 1954
petrol oil	1.9–2.22	1 MHz–1 GHz	liquid		von Hippel 1954
poly(2-hydroxyethyl methacrylate)	1.5–3.0	10 MHz–1 GHz	hydrogel	213–253 K	Xu, Vij & McBrierty 1994

This paper has been typeset from a Microsoft Word file prepared by the author.